Journal of Power Sources 195 (2010) 7370–7374

Contents lists available at ScienceDirect

Journal of Power Sources

journal homepage: www.elsevier.com/locate/jpowsour

Short communication

Oxidation behavior and electrical property of ferritic stainless steel interconnects with a Cr–La alloying layer by high-energy micro-arc alloying process

Z.J. Feng, C.L. Zeng*

State Key Laboratory for Corrosion and Protection, Institute of Metal Research, Chinese Academy of Sciences, 62 Wencui Road, Shenyang 110016, China

ARTICLE INFO

Article history:
Received 21 April 2010
Received in revised form 2 June 2010
Accepted 2 June 2010
Available online 10 June 2010

Keywords:
Solid oxide fuel cells
Ferritic metallic interconnect
High-energy micro-arc alloying technique
Lanthanum chromite
Oxidation
Contact resistance

ABSTRACT

Chromium volatility, poisoning of the cathode material and rapidly decreasing electrical conductivity are the major problems associated with the application of ferritic stainless steel interconnects of solid oxide fuel cells operated at intermediate temperatures. Recently, a novel and simple high-energy micro-arc alloying (HEMAA) process is proposed to prepare $LaCrO_3$-based coatings for the type 430 stainless steel interconnects using a $LaCrO_3$–Ni rod as deposition electrode. In this work, a Cr–La alloying layer is firstly obtained on the alloy surface by HEMAA using Cr and La as deposition electrode, respectively, followed by oxidation treatment at 850 °C in air to form a thermally grown $LaCrO_3$ coating. With the formation of a protective scale composed of a thick $LaCrO_3$ outer layer incorporated with small amounts of Cr-rich oxides and a thin Cr_2O_3-rich sub-layer, the oxidation rate of the coated steel is reduced remarkably. A low and stable electrical contact resistance is achieved with the application of $LaCrO_3$-based coatings, with a value less than 40 mΩ cm^2 during exposure at 850 °C in air for up to 500 h.

1. Introduction

The development of intermediate temperature solid oxide fuel cells (SOFCs) has made it possible to replace ceramic interconnects with high temperature alloys. Among these alloys, ferritic stainless steels, usually chromia-forming alloys, have been most widely studied for interconnect applications [1–3], due to their excellent thermal expansion coefficient compatibility with other ceramic components, excellent electric and thermal conductivity, mechanic properties and relatively low cost. However, the oxidation of stainless steels at the operating temperatures of SOFCs (e.g., 750–850 °C) in the cathode side still causes serious problems, including the poisoning of the cathode material due to chromium evaporation into the cathode and the increase in electric contact resistance owing to the growth of oxide scale [4,5]. As a result, the lifetime of cell stacks is significantly reduced. The oxide scale formed on ferritic stainless steels is usually composed of two layers, a Mn–Cr spinel outer layer and a chromia subscale [6]. Alloy or surface modifications and the application of protective conductive coatings have been attempted to eliminate these problems [7–11]. Recent studies have been concentrated on developing coatings for metallic interconnects. Perovskite oxides, such as (La, Sr)CrO_3 and (La, Sr)MnO_3, have been extensively investigated as protective coatings for ferritic stainless steels interconnect due to their high electrical conductivity, thermal compatibility and stability in the oxidizing environments [11–19]. Numerous techniques have been developed to deposit perovskite coatings on stainless steel substrate, such as sputtering [15], screen-printing [16], sol–gel [17], electrodeposition [18] and plasma spraying [19].

Recently, a novel and simple process based on high-energy micro-arc alloying (HEMAA) has been considered to directly deposit compact oxide coatings on ferritic stainless steels [20] by the authors' group. HEMAA is a micro welding technique using short-duration and high-current electrical pulses to deposit an electrode material on a metallic substrate, and thus normally can produce high-quality diffusion coatings at a lower cost, with a minimal thermal distortion or microstructural changes of the substrate due to low-energy transfer involved in the HEMAA process. In the authors' previous work [20], a $LaCrO_3$-based coating has been deposited successfully on the type 430 stainless steel by HEMAA using a $LaCrO_3$–Ni electrode, with a good oxidation resistance and a low electrical contact resistance. However, some micro-pores are present at the oxide layer/substrate alloy interface after oxidation. It is noted that it is much difficult to deposit an oxide coating by HEMAA than a metallic coating due to the high brittleness of oxide electrodes used for deposition. The addition of some metallic particles to $LaCrO_3$ electrode helps to decrease its brittleness, thus producing a more adhesive coating.

Some studies indicated that La coatings [21] prepared by electron beam vacuum deposition and La_2O_3 coatings by sol–gel method [22,23] react with the thermally grown Cr_2O_3 to form $LaCrO_3$ upon thermal exposure. Thus, the present authors consider that it may be a preferred method to deposit firstly a Cr–La alloy-

* Corresponding author. Tel.: +86 24 23904553; fax: +86 24 23893624.
E-mail address: clzeng@imr.ac.cn (C.L. Zeng).

0378-7753/$ – see front matter © 2010 Elsevier B.V. All rights reserved.
doi:10.1016/j.jpowsour.2010.06.016

ing layer on ferritic stainless steels by HEMAA, followed by heat treatment in air to form a dense thermally grown $LaCrO_3$ layer.

2. Experimental

Type 430 ferritic stainless steel (430SS) was used as the substrate alloy. The steel plates were cut into pieces with the size of 10 mm × 10 mm × 1.5 mm, followed by grinding with 150-grit SiC paper and degreasing with acetone.

A pure chromium rod and a pure lanthanum rod were used, respectively, as deposition electrode to deposit Cr and La on 430SS to form a Cr–La alloying layer on all sides of the specimens. The details for the coating process are as follows. Chromium was firstly deposited on the specimen surface with a succession of high-energy pulse discharge depositing operation, followed by lanthanum with a succession of low-energy pulse discharge depositing operation, and chromium again with a succession of high-energy pulse discharge depositing operation. To avoid heating and oxidation during deposition, the substrate area was kept at room temperature by a strong jet of argon gas.

The coated and uncoated samples contained in alumina crucibles were put into high temperature furnace for oxidation treatment at 850 °C in air for up to 200 h immediately after the coating process was finished. To determine the oxidation kinetics the crucibles containing the samples were removed out of the furnace every 20 h, cooled to room temperature in air, weighed, and then put into the furnace again for further oxidation.

The electrical contact resistances of the uncovered and covered steels were measured using a setup shown in Fig. 1. Both surfaces of the samples pre-oxidized at 850 °C in air for various lengths of time were covered by platinum paste, and then platinum foils were placed on the top of the pastes as current collectors. Pt wires as electric leads were spot-welded to the sides of Pt foils and the resulting resistance was subtracted from the original results. All the electrical contact resistance measurements were conducted at 850 °C in air.

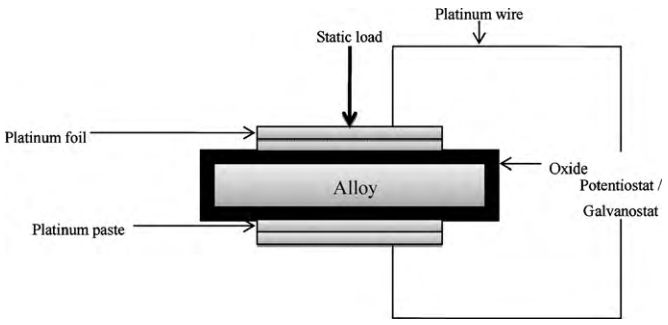

Fig. 1. Schematic setup for area-specific contact resistance measurements.

X-ray diffraction (XRD) was conducted to analyze the samples using PANalytical diffractometer (X' Pertpro) with Cu k_a radiation source. The XRD analysis was operated at 40 kV. Scanning electron microscope (SEM) used for the purpose of imaging and microanalysis is a FEI Inspect F SEM equipped with an Oxford energy dispersive X-ray (EDX) microanalysis.

3. Results and discussion

3.1. Oxidation behavior for uncovered and covered samples

During deposition of Cr and La by HEMAA, mass transfer occurs, i.e. Cr and La transfer from Cr and La electrodes to the alloy sur-

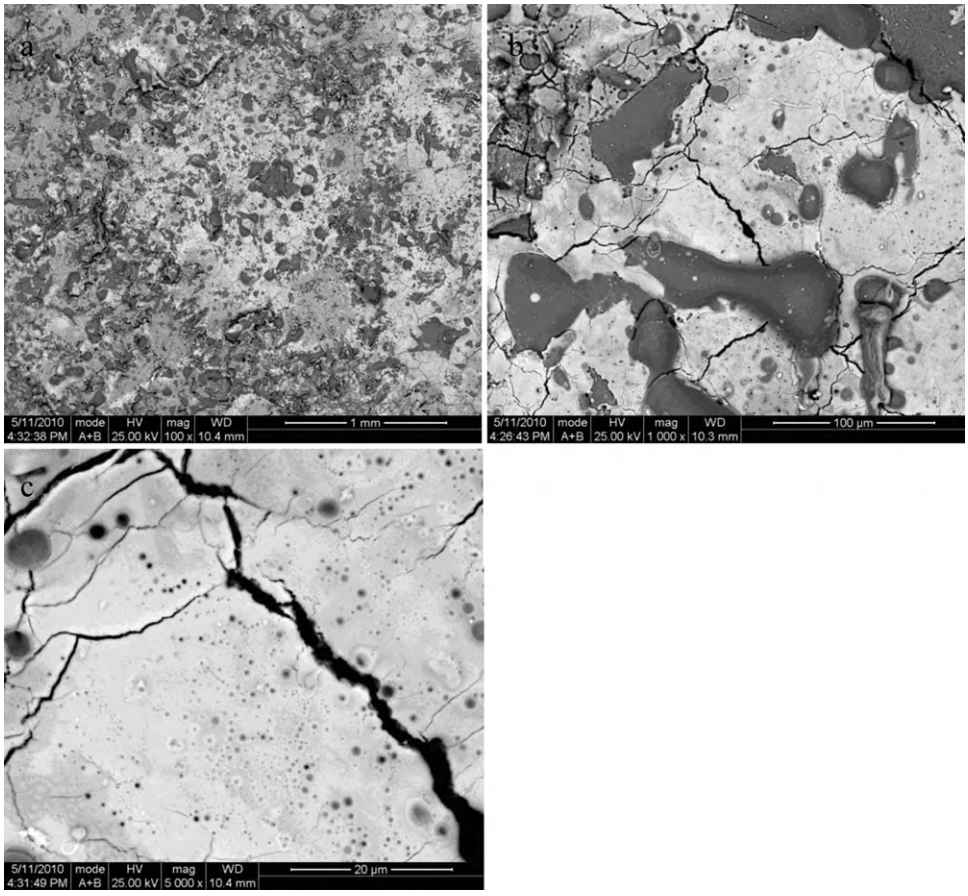

Fig. 2. Back-scattered surface morphologies of the as-deposited Cr–La alloying layer. (a) General view; (b) and (c) the amplified views of (a).

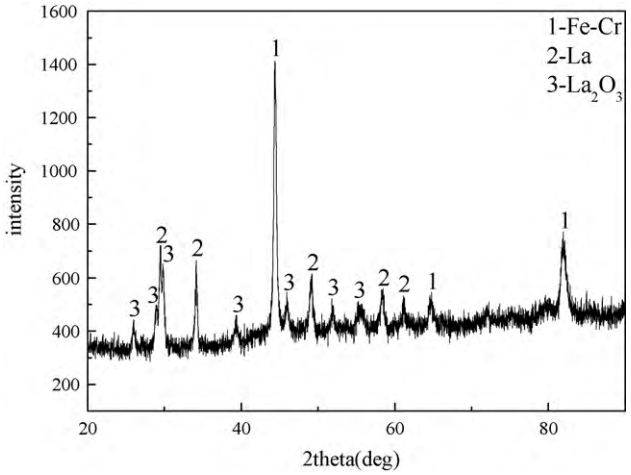

Fig. 3. X-ray diffraction pattern for the as-deposited Cr–La coating.

face, and some elements such as Cr and Fe from the substrate alloy to the electrodes. This gives rise to the formation of a Cr–La alloying layer on 430SS. Fig. 2 shows the back-scattered surface morphologies of the as-deposited Cr–La alloying layer. The Cr–La alloying layer is composed of white phases and dark phases, among which the white phases occupy a higher surface area than the darks phases. Furthermore, the white phases are incorporated with some small dark phases (Fig. 2b and c). EDAX analysis indicated that the white phases contain 54La–26Cr–7Fe–13O (in wt.%), while the dark phases contain 3La–65Cr–27Fe–5O. Additionally, some cracks were also observed. XRD analysis (Fig. 3) indicates that the as-deposited Cr–La alloying layer is composed of Fe–Cr, La and La_2O_3. Cr–La binary alloy phase diagram (Fig. 4) [24] shows that Cr–La alloy exhibits two-phase microstructure composed of Cr and La, which is close to the experimental observation. The phase La_2O_3 probably results from the oxidation of La during HEMAA process and also from the oxidation of Cr–La layer at room temperature in air, because La has a high affinity for oxygen. Additionally, during deposition process La together with La_2O_3 existing on the surface of La electrode was transferred from the electrode to the alloy surface. It should be noted that the as deposited Cr–La layer would pest quickly in air at room temperature. This kind of pesting phenomenon is related to the fast oxidation of La. This result suggests that La is enriched in the external part of Cr–La Layer to a certain extent, just as shown in Fig. 2. The microstructure of the as

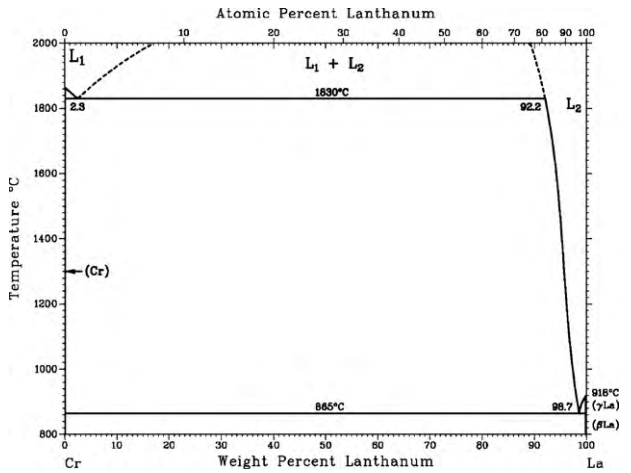

Fig. 4. Binary phase diagram of Cr–La.

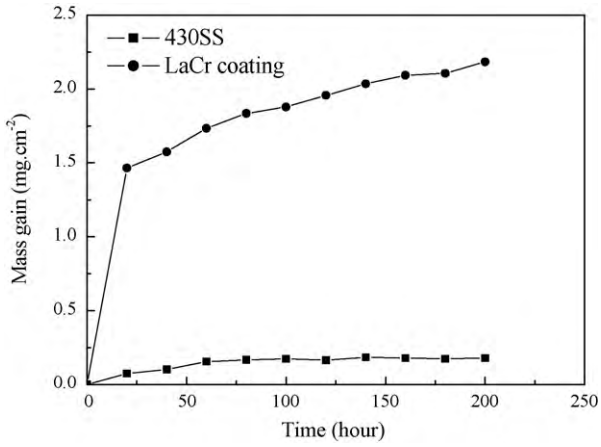

Fig. 5. Oxidation kinetics for the uncovered and covered 430 stainless steel at 850 °C in air.

deposited Cr–La layer was not examined because of the pesting problem.

Thus, to avoid the pesting phenomenon the Cr–La coated specimens were put into a high temperature furnace for oxidation treatment at 850 °C in air immediately after deposition. Fig. 5 shows the mass gain versus time curves for the uncovered and the covered steel at 850 °C in air. In the initial 20 h, the mass for the coated steel increased instantly with time due to rapid oxidation of La and Cr. With extended exposure, the coated steel followed approximately a parabolic oxidation law, with a significantly decreased oxidation rate. Unlike the covered steel, the bare steel followed an approximate parabolic oxidation law, with a much lower mass gain than the covered steel.

3.2. Oxidation products

Fig. 6 shows the XRD pattern of the Cr–La coated steel after oxidation at 850 °C in air for 20 h. The oxide scale formed on the coated steel is mainly composed of perovskite $LaCrO_3$ with small amounts of complex oxide $(Cr,Fe)_2O_3$. It is clear that the perovskite oxide $LaCrO_3$ can be formed quickly by the solid reaction between La_2O_3 and Cr_2O_3 at 850 °C.

From the back-scattered cross-sectional morphology of the covered steel oxidized at 850 °C for 20 h (Fig. 7b), it is seen that the oxide scale exhibits bi-layered microstructure composed of a thick bright $LaCrO_3$ outer layer incorporated with small amounts of gray

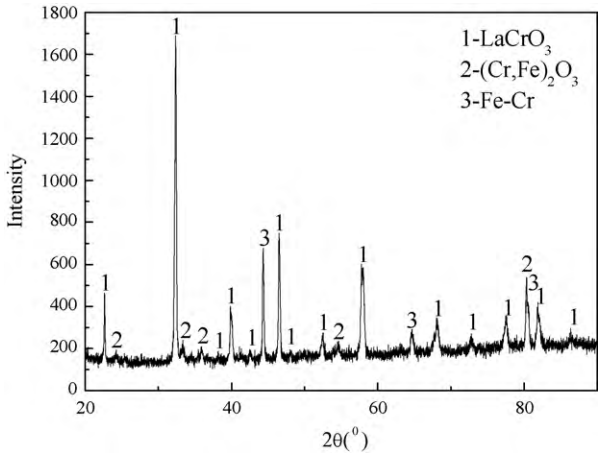

Fig. 6. X-ray diffraction pattern for the Cr–La coated steel after oxidation at 850 °C in air for 20 h.

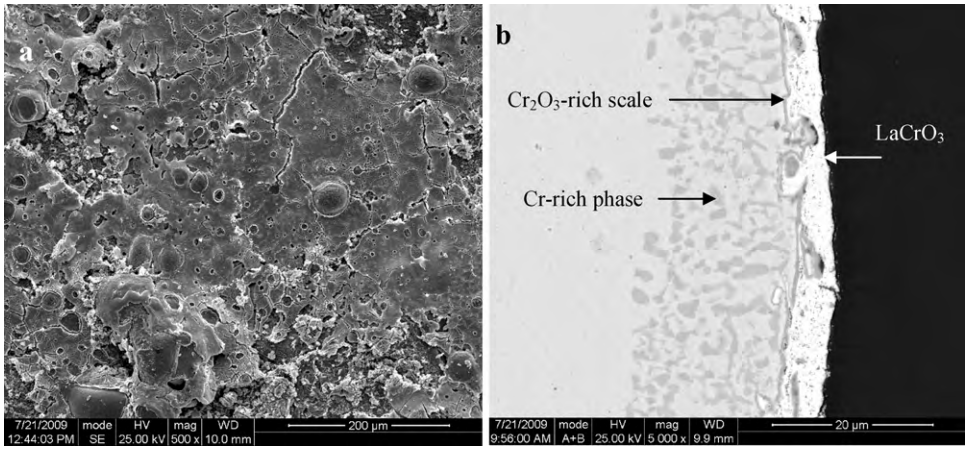

Fig. 7. Surface (a) and cross-sectional (b) morphologies of the Cr–La coated steel after oxidation at 850 °C in air for 20 h.

(Cr, Fe)-rich oxides ($(Cr,Fe)_2O_3$), and a thin Cr_2O_3-rich inner layer, identified by XRD and EDAX. EDAX analysis indicated the bright $LaCrO_3$ layer was also doped with around 1% Fe (in wt.%). Beneath the oxide scale is a wide Cr-rich region, where many gray Cr-rich metallic phases are distributed over the bright substrate alloy with a higher Cr content than the as-received alloy. The oxidation process at 850 °C gives rise to the precipitation of some Cr-rich phases in the Cr-alloying layer produced by HEMAA. The presence of a Cr-rich layer is helpful to the formation of a Cr_2O_3-rich scale at the $LaCrO_3$ layer/substrate alloy interface. In addition, some pores are present in the coating. These pores mainly result from HEMAA process.

Fig. 8 shows the XRD pattern for the coated steel after oxidation at 850 °C for 200 h. The scale still mainly consists of $LaCrO_3$ with small amounts of complex oxide $(Cr,Fe)_2O_3$. Fig. 9 shows the cross-sectional morphology of the coated steel after oxidation for 200 h. Though the coating is significantly thicker than that oxidized for 20 h due to the manual deposition of coatings, the oxide scale still shows bi-layered microstructure with a $LaCrO_3$ outer layer and a Cr_2O_3-rich inner layer, as observed for 20 h oxidation.

Through the mass transfer between the deposition electrode and the substrate alloy, HEMAA process produces a Cr–La alloying layer mainly containing Cr, La and Fe, among which La is abundantly present in the outer region. La-based perovskite oxides such as $LaCrO_3$ are thermodynamically more stable than some individual metal oxides such as Fe_2O_3. During heat treatment at 850 °C in air, La and Cr were oxidized to form perovskite oxide $LaCrO_3$ doped with small amounts of Fe, as observed in the experiments. Fe which did not react with La could react with Cr to form some complex oxides $(Cr,Fe)_2O_3$. Meanwhile, a continuous thin Cr_2O_3-rich scale was formed along the substrate/$LaCrO_3$ layer interface. This bi-layered scale composed of external $LaCrO_3$ and inner Cr_2O_3 possess an excellent protectiveness to the substrate alloy.

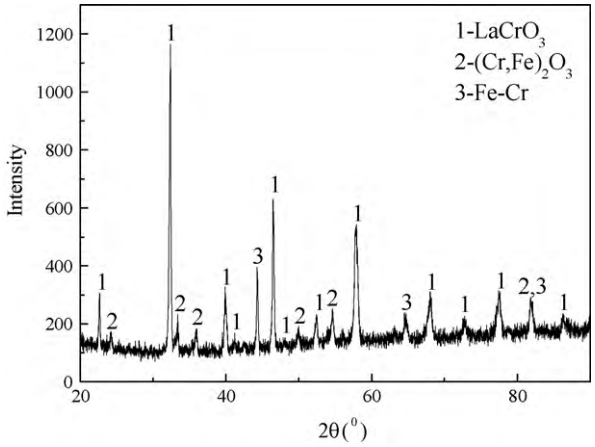

Fig. 8. X-ray diffraction pattern for the Cr–La coated steel oxidized at 850 °C in air for 200 h.

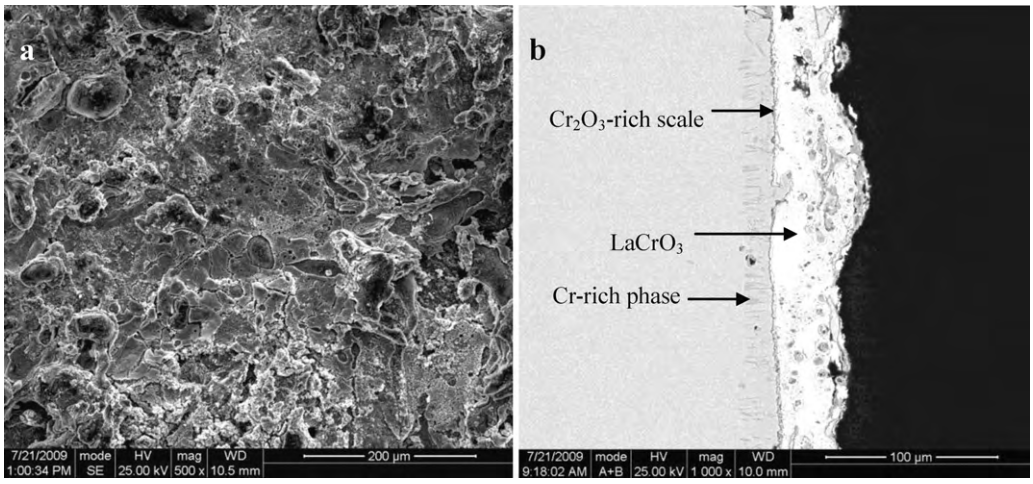

Fig. 9. Surface (a) and cross-sectional (b) morphologies of the Cr–La coated steel after oxidation at 850 °C in air for 200 h.

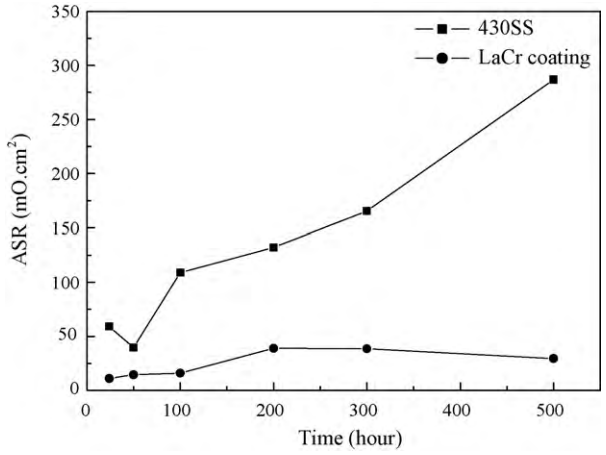

Fig. 10. Electrical contact resistance versus time curves for the covered and uncovered steel at 850 °C in air.

3.3. Electrical contact resistance measurements

The area-specific resistance (ASR) of the covered and uncovered specimens, pretreated at 850 °C in air for various lengths of time, was measured at 850 °C in air, as shown in Fig. 10. ASR for the uncoated steel at 850 °C in air increases from around 60 mΩ cm^2 to 288 mΩ cm^2 after oxidation at 850 °C for 24 h and 500 h, respectively. ASR for the coated steels fluctuates slightly with time up to 500 h, but with a value less than less 40 mΩ cm^2. These values are significantly smaller than those for the uncovered steel, especially after oxidation for a longer time. The fluctuation of ASR for the coated steel is mainly related to using different specimens for every ASR measurement, because manual HEMAA operation produced Cr–La alloying layers with a varying thickness. As a result, the thickness for the thermally grown $LaCrO_3$ layer on the Cr–La coated specimens after oxidation treatment for various times is different. It was also found that the thickness of the inner Cr_2O_3-rich scale increased slightly with time. ASR is proportional to the thickness of oxide scale, i.e. the thickness of outer $LaCrO_3$ layer and inner Cr_2O_3 layer. The generally accepted upper limit of ASR for SOFC interconnects is 0.1 Ω cm^2 [25]. It is clear that the thermally grown oxide scale possesses a good protectiveness to the substrate steel, with an acceptable electrical contact resistance.

4. Conclusions

A novel and simple high-energy micro-arc alloying process has been used successfully to prepare $LaCrO_3$-based coatings for the type 430 stainless steel interconnects of solid oxide fuel cells. To obtain a thermally grown $LaCrO_3$, a Cr–La alloying layer was firstly obtained on the alloy surface by HEMAA using Cr and La as deposition electrode, respectively, followed by oxidation treatment at 850 °C in air. The oxidation treatment gave rise to the formation of a compact and protective oxide coating with a bi-layered microstructure composed of a thick $LaCrO_3$ external layer formed by the solid reaction between the thermally grown Cr_2O_3 and La_2O_3 and a thin Cr_2O_3 inner layer on the coated steel, which thereby possesses an excellent protectiveness to the substrate alloy. Moreover, compared with the uncoated steel a low and stable electrical contact resistance with a value less than 40 mΩ cm^2 was achieved with the application of $LaCrO_3$-based coatings during exposure at 850 °C in air for up to 500 h.

Acknowledgement

The project supported by National Natural Science Foundation of China, Grant No 50771101.

References

[1] Z. Yang, K.S. Weil, D.M. Paxton, J.W. Stevenson, J. Electrochem. Soc. A 1188 (2003) 150A.
[2] J. Rufner, P. Gannon, P. White, M. Deibert, S. Teintze, R. Smith, H. Chen, Int. J. Hydrogen Energy 33 (2008) 1392.
[3] J.E. Hammer, S.J. Laney, R.W. Jackson, K. Coyne, F.S. Pettit, G.H. Meier, Oxid. Met. 1 (2007) 67.
[4] S.P.S. Badwal, R. Deller, K. Foger, Y. Ramprakash, J.P. Zhang, Solid State Ionics 99 (1997) 297–310.
[5] Y. Matsuzaki, I. Yasuda, Solid State Ionics 132 (2000) 271–278.
[6] Z. Yang, Int. Mater. Rev. 53 (2008) 39–54.
[7] T. Horata, Y. Xiong, K. Yamaji, N. Sakai, H. Yokokawa, Fuel cells 2 (2–30) (2002) 189–194.
[8] P.Y. Hou, J. Stringer, Mater. Sci. Eng. A 202 (1995) 1–10.
[9] S. Chevalier, J.P. Larpin, Acta. Mater. 50 (2002) 3105–3114.
[10] J.W. Wu, C.D. Johnson, R.S. Germmen, X.B. Liu, J. Power Sources 189 (2009) 1106–1113.
[11] S. Linderoth, Surf. Coat. Technol. 80 (1996) 185.
[12] C. Johnson, R. Gemmen, N. Orlovskaya, Composite B 35 (2004) 167–172.
[13] Y.D. Zhen, S.P. Jiang, S. Zhang, V. Tan, J. Eur. Ceram. Soc. 26 (2006) 3253–3264.
[14] C Johnson, N. Orlovskaya, A. Coratolo, C. Cross, J.W. Wu, R. Germmen, X.B. Liu, Int. J. Hydrogen Energy 34 (2009) 2408–2415.
[15] Z. Yang, G. Xia, G.D. Maupin, J.W. Stevenson, J. Electrochem. Soc. 153 (2006) A1852.
[16] T. Brylewski, K. Przybylski, J. Morgiel, Mater. Chem. Phys. 81 (2003) 434.
[17] J.H. Zhu, Y. Zhang, A. Basu, Z.G. Lu, M. Parathaman, D.F. Lee, E.A. Payzant, Surf. Coat. Technol. 177 (2004) 65.
[18] N. Shaigan, D.G. Ivey, W. Chen, J. Electrochem. Soc. 155 (2008) D278–D284.
[19] H.W. Nie, T.L. Wen, H.Y. Hu, Mater. Res. Bull. 38 (2003) 1531.
[20] Z.J. Feng, C.L. Zeng, J. Power Sources 195 (2010) 4242–4246.
[21] N. Oishi, T. Namikawa, Y. Yamazaki, Surf. Coat. Technol. 132 (2000) 58–64.
[22] J.S. Yoon, J. Lee, H.J. Hwang, et al., J. Power Sources 181 (2008) 281.
[23] Z. Lu, J. Zhu, Y. Pan, N. Wu, A. Ignatiev, J. Power Sources 178 (2008) 282–290.
[24] Binary Alloy Phase Diagrams, ASM, 1986.
[25] W.Z. Zhu, S.C. Deevi, Mater. Sci. Eng. A 348 (2003) 227–243.